International Journal of Impact Engineering 38 (2011) 171–180

Contents lists available at ScienceDirect

International Journal of Impact Engineering

journal homepage: www.elsevier.com/locate/ijimpeng

About the dynamic uniaxial tensile strength of concrete-like materials

Y.B. Lu [1], Q.M. Li*

School of Mechanical, Aerospace and Civil Engineering, Pariser Building, The University of Manchester, Sackville Street, Manchester M13 9PL, UK

ARTICLE INFO

Article history:
Received 6 September 2009
Received in revised form
20 October 2010
Accepted 23 October 2010
Available online 11 November 2010

Keywords:
Concrete-like material
Tensile strength
Dynamic increase factor
Strain-rate effect

ABSTRACT

Experimental methods for determining the tensile strength of concrete-like materials over a wide range of strain-rates from 10^{-4} to $10^{2}\,s^{-1}$ are examined in this paper. Experimental data based on these techniques show that the tensile strength increases apparently with strain-rate when the strain-rate is above a critical value of around 10^{0}–$10^{1}\,s^{-1}$. However, it is still not clear that whether the tensile strength enhancement of concrete-like materials with strain-rate is genuine (i.e. it can be attributed to only the strain-rate effect) or it involves "structural" effects such as inertia and stress triaxility effects. To clarify this argumentation, numerical analyses of direct dynamic tensile tests, dynamic splitting tests and spalling tests are performed by employing a hydrostatic-stress-dependent macroscopic model (K&C concrete model) without considering strain-rate effect. It is found that the predicted results from these three types of dynamic tensile tests do not show any strain-rate dependency, which indicates that the strain-rate enhancement of the tensile strength observed in dynamic tensile tests is a genuine material effect. A micro-mechanism model is developed to demonstrate that microcrack inertia is one of the mechanisms responsible for the increase of dynamic tensile strength with strain-rate observed in the dynamic tensile tests on concrete-like materials.

1. Introduction

Concrete-like materials (e.g. mortar, concrete and geo-materials) have been widely used in civil and military engineering structures, which may be threatened by intensive dynamic loads (e.g. explosion and impact). Dynamic strengths of concrete-like materials are frequently required in the design and modelling of these structures. Two important parameters in a dynamic strength model are dynamic uniaxial tensile and compressive strengths. The former controls the tensile failure (e.g. spalling, scabbing and fragmentation) while the latter is responsible for the compressive resistance (e.g. penetration and perforation) when the structure made of concrete-like materials responds to impact or blast loading.

It has been observed that both the tensile and compressive strengths of concrete-like materials increase with strain-rate, especially when the strain-rate is greater than a transition strain-rate, which is around 10^{0}–$10^{1}\,s^{-1}$ for uniaxial tension and $10^{2}\,s^{-1}$ for uniaxial compression, respectively. However, it has been found that the strain-rate enhancement of the compressive strength of concrete-like materials is largely caused by the introduction of radial confinement in split Hopkinson pressure bar (SHPB) tests [1–6], which cannot be simply interpreted as material behaviour. A similar argument was made by Cotsovos and Pavlović [7] for the dynamic tensile strength of concrete, i.e. the tensile strength enhancement of concrete based on direct dynamic tensile tests was caused by axial inertial effects, and thus, represents a "structural" effect. Cotsovos and Pavlović's [7] conclusion, however, is in contradiction with the findings in Hentz et al. [2] that the dynamic tensile strength based on spalling tests represented the material-intrinsic behaviour of concrete. In spite of these different opinions on the dynamic tensile strength of concrete-like materials, experimental results consistently demonstrate the strong strain-rate dependence of the tensile strength when the strain-rate is above a transition strain-rate, which will be shown with further details in Section 2. Therefore, it is necessary to answer following two questions, i.e. (i) can the observed dynamic tensile strength enhancement of concrete-like materials be attributed to strain-rate effect, and (ii) is it necessary to consider the dynamic tensile strength enhancement in the dynamic strength model of concrete-like materials.

Available experimental methods for the measurement of tensile strength of concrete-like materials are examined in Section 2. Stress states in three types of dynamic tensile tests (i.e. direct dynamic tensile test, dynamic splitting test and spalling test) are calculated in Section 3 based on a macroscopic hydrostatic-stress-dependent material model where the material behaviour is assumed to be strain-rate-independent. It is shown that the effect

* Corresponding author. Tel.: +44 1613065740; fax: +44 1613063849.
E-mail address: qingming.li@manchester.ac.uk (Q.M. Li).
[1] Present address: School of Manufacturing Science and Engineering, Southwest University of Science and Technology, Mianyang 621010, Sichuan, PR China.

0734-743X/$ – see front matter © 2010 Elsevier Ltd. All rights reserved.
doi:10.1016/j.ijimpeng.2010.10.028

of non-uniaxial stress state on tensile strength enhancement is negligibly small, which supports findings in Hentz et al. [2]. Thus, the increase of dynamic tensile strength of concrete-like materials at the macroscopic level is primarily attributed to the influence of strain-rate. Based on a micro-mechanism model, it is found in Section 4 that the microcrack inertia is one of the mechanisms responsible for the dynamic tensile strength enhancement of concrete-like materials observed in dynamic tensile tests. Conclusions are presented in Section 5.

2. Tensile tests of concrete-like materials

2.1. Quasi-static tensile tests

In order to establish a reference for the study of the dynamic tensile strength of concrete-like materials, quasi-static tensile tests are required. Three testing methods are generally accepted to measure the quasi-static tensile strength of concrete-like materials, i.e. the direct tensile test, the modulus of rupture test and the splitting (or Brazilian) test [8]. In a direct tensile test, a specimen is gripped at its two ends and pulled apart in tension where the tensile strength is calculated by dividing the load at failure over the cross-sectional area of the specimen, which can be performed up to strain-rate of $10^{-1}\ s^{-1}$ on a universal loading machine. For the modulus of rupture test, a rectangular beam is loaded at the mid-point up to the bending failure, from which the maximum tensile flexural stress calculated at failure is called the modulus of rupture and is considered to represent the tensile strength. In a splitting test, a cylindrical specimen is positioned such that its longitudinal axis lies horizontally between the loading platens in different ways [Fig. 1(a–c)]. The load applied through bearing stripes is increased until the specimen is split along its vertical axis by tension due to the much smaller tensile strength of concrete-like materials than their corresponding compressive strength.

Researchers have indicated that, among the three testing methods, the splitting test gives the most accurate measurement of the true tensile strength of concrete-like materials in a wide range of strain-rates from $10^{-7}\ s^{-1}$ to about $10^{0}\ s^{-1}$ (e.g. [9]). Difficulties are encountered in the direct tensile tests when it requires a pure tensile force free of eccentricity. Often, when grips are used to anchor the specimen, compression from the grips is combined with tension from the testing machine. This particular combination of forces has been shown to result in failure at stress levels below the maximum tensile strength [10]. Although the modulus of rupture test is easier to conduct than the direct tensile test, it tends to overestimate the tensile strength [11] as a result of the assumption that there is always a linear distribution of stress on the cross-section of the beam whereas the actual stress distribution becomes parabolic when the failure load is approached [8].

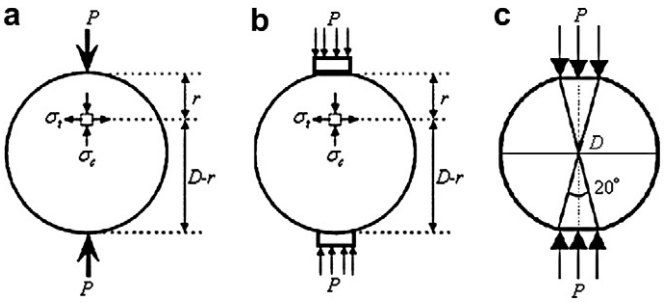

Fig. 1. Schemes of the splitting test, (a) when concentrated line load is applied, (b) with bearing strips, and (c) diametric compression on the flattened Brazilian cylinder.

The stress state of the splitting test has an analytical solution if a plane-strain state is assumed and a concentrated line load is applied [12]. The stresses associated with such loading configuration are illustrated in Fig. 1(a). When the compressive load, P, is applied to the specimen, points located near the centre of the cylinder along its vertical diameter are subjected to a vertical compressive stress of [9]

$$\sigma_c = \frac{2P}{\pi BD}\left[\frac{D^2}{r(D-r)} - 1\right] \tag{1}$$

where B is the length of the cylinder, D is its diameter, and r is the distance from the point on the vertical diameter to the top of the cylinder. This point is subjected to a horizontal tensile stress as well, whose magnitude is equal to [9]

$$\sigma_{ts} = \frac{2P}{\pi BD} \tag{2}$$

In an actual splitting test, the load is applied through a relatively small zone, as shown in Fig. 1(b). For concrete-like materials, this zone is usually controlled using bearing strips that spread the load to the actual loading–bearing width. The tensile strength determined from tests conducted without the bearing strips is typically about 8% lower than that recorded by tests conducted with the bearing strips [9]. ASTM [11] recommended that the width of the strips (b) should be approximately 1/12 of the diameter of the cylinder (D). A modified expression to measure the tensile strength is proposed [12],

$$\sigma_{ts} = \frac{2P}{\pi BD}\left(1-\beta^2\right)^{3/2} \tag{3}$$

where $\beta = b/D$ is the relative width of the load-bearing strips.

Wang et al. [13] employed flattened cylindrical specimens to perform Brazilian tests [Fig. 1(c)]. The tensile strength with flat angle of 20° can be estimated by the following expression

$$\sigma_{ts} = 0.95\frac{2P}{\pi BD}. \tag{4}$$

It is worth noting that Eqs. (2–4) can only be used to calculate the maximum tensile stress. Strain at failure and the stress–strain relationship before failure cannot be obtained from splitting tests.

2.2. Dynamic tensile tests

The splitting test technique has been used to test brittle materials when loading conditions belong to quasi-static or low strain-rates. The loading process has been modelled by different researchers and the testing results have been justified (e.g. [12]). It has been recently brought into use for measuring the dynamic tensile strength of concrete-like materials at intermediate strain-rates. The SHPB is used for dynamic splitting tests, as illustrated in Fig. 2. The dynamic tensile strength, σ_{td}, of the splitting cylinder is proportional to the average of input and output force histories (P_t) through a modification of Eq. (4), which is expressed as [13]

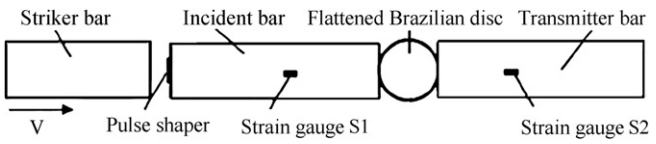

Fig. 2. The side view of a dynamic splitting test arrangement in the SHPB [13].

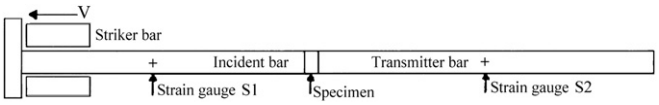

Fig. 3. The schematic illustration of a tensile Hopkinson bar set-up [20].

$$\sigma_{td} = 0.95\frac{2P_t}{\pi BD}, \quad P_t = \frac{1}{2}(P_1 + P_2) \tag{5}$$

where P_1 and P_2 are the total axial forces on the interfaces between the incident bar and specimen and between the transmitter bar and specimen, respectively. Because of the stress wave propagation in the specimen, P_2 has a time lag of t_0 ($t_0 \approx D/c_s$ with c_s being the uniaxial stress wave speed in the specimen). The advantage of using force histories of P_1 and P_2 in numerical simulations is that there is no need to shift the strain gauge signals on pressure bars to the specimen interface and to correct wave dispersion.

The strain-rate in the specimen is not a constant during the effective loading period. However, it has been shown that there exists a linear correlation between different measures of the representative strain-rates in SHPB tests of concrete-like materials [4]. Therefore, the selection of a particular representative strain-rate measure does not influence the objective of this study. The representative strain-rate used by Tedesco and Ross [8] in the dynamic tensile test will be adapted, i.e.

$$\dot{\varepsilon}_z = \frac{\sigma_{td}}{E_s T} \tag{6}$$

where T is the time lag between the start of the transmitted stress wave and the occurrence of the maximum transmitted stress, which is determined from P_2 history. E_s is the quasi-static Young's modulus of the specimen. It has been shown that the elastic moduli are not particularly strain-rate sensitive comparing with the strain-rate sensitivity of tensile strength (e.g. [14,15]), therefore, the quasi-static Young's modulus is used in Eq. (6).

There are various set-ups of direct dynamic tensile tests, e.g. [16–20]. We will employ Tedesco et al.'s [20] set-up shown in Fig. 3 in the numerical tests in Section 3 for its simplicity. Direct dynamic tensile test techniques are suitable for strain-rates between 10^{-1} and 10^{1} s^{-1} [14,21].

Direct dynamic tensile tests are used to measure the tensile strength of brittle materials in the strain-rate range from 10^{0} s^{-1} to about 20 s^{-1} [22]. The average tensile stress (σ_{td}) and strain-rate ($\dot{\varepsilon}_z$) in the specimen are

$$\sigma_{td} = \frac{P_1 + P_2}{2A_s} \tag{7a}$$

$$\dot{\varepsilon}_z = \frac{V_1 - V_2}{L_0} \tag{7b}$$

where A_s is the cross-sectional area (within the gauge length) of the specimen; V_1 and V_2 are the average particle velocities on the two ends of the specimen, respectively; L_0 is the gauge length of the specimen. Because of the complexity of the specimen shape (i.e. dumbbell shape) and the requirement of ensuring connection (e.g. by bond, screw or clamp) between the specimen and the pressure bars, uniaxial stress condition in the specimen in a tensile Hopkinson bar test may be violated and connection between the specimen and the pressure bars may be failed, which will influence the accuracy of the testing results.

To achieve higher strain-rates in dynamic tensile tests of brittle materials, other experimental techniques have been developed. One of them is the spalling test based on London and Quinney's [23] work, which can achieve strain-rates in the order of 10^{2} s^{-1} for brittle specimens that have a much higher compressive strength than tensile strength to avoid the pre-damage by the compressive stress wave. The schematic layout of a spalling test set-up is shown in Fig. 4, which consists of a cylindrical striker launched by an air gun, an instrumented pressure bar as a measuring transducer, and a long cylindrical specimen in contact with the bar. When the striker hits the pressure bar, an elastic compression wave is generated and then transmitted into the specimen with a small part reflected back into the pressure bar. The compressive wave is reflected in tension causing the fracture of the specimen at a specific distance from its free end. The impact speed of the striker should be smaller than a critical value to ensure that the specimen does not suffer any compressive damage when the compressive stress wave passes through the specimen. With the strain-time signals recorded by strain gauges, the dynamic tensile strength of the specimen can be evaluated by the superposition of the compression and tension waves at the first rupture position [24,25]. A more detailed description of this experimental technique can be found in Ref. [26]. It is obvious that this experimental set-up avoids difficulties of specimen connections in a tensile Hopkinson bar experiment. However, whether the uniaxial stress condition is satisfied in the specimen in spalling tests should be examined. The dynamic tensile strength in a spalling test can be measured directly from the average particle velocity at the free surface of specimen, which can be expressed as [14],

$$\sigma_{td} = \frac{1}{2}\rho_s L\frac{\delta u_{pb}}{\delta t} \tag{8}$$

in which ρ_s is the density of the specimen material; L is the original length of specimen; δt is the time interval that the wave needs to propagate from the beginning to the end of the specimen; δu_{pb} is the 'pull-back' velocity determined from the particle velocity history as illustrated later in Fig. 13. The data of δt and δu_{pb} can also be obtained through experimental methods as described in Ref. [14]. However, if they are not available, procedures which are more complicated than Eq. (8) such as those proposed in Refs. [25,26] can be used for calculating the dynamic tensile strength from spalling tests. The strain-rate is obtained from the evolution of the stress in the location of the tensile crack by [24]

$$\dot{\varepsilon}_z = \frac{\sigma_{td}}{E_s t_c}, \tag{9}$$

where t_c is the critical time determined from the beginning of the specimen loading up to fracture.

It should be realised that the definitions of strain-rate are different for the above three types of dynamic tensile testing techniques. For dynamic splitting tests and spalling tests, strain-rate is defined as the peak strain divided by a time interval between the start of loading and specimen failure (nominal strain-rate). For tensile Hopkinson bar tests, the representative strain-rate is taken as the strain-rate associated with the ultimate tensile strength.

2.3. The dynamic tensile strength enhancement of concrete-like materials

It has been generally accepted that there is an apparent increase of the dynamic strength when concrete-like materials is subjected to high strain-rates. The effect of strain-rate on the compressive or

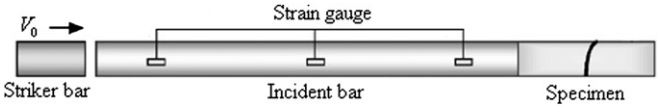

Fig. 4. The scheme of a spalling test set-up [25].

tensile strength of concrete-like materials is typically reported as a dynamic increase factor (DIF) (i.e. the ratio of dynamic to quasi-static strength) versus strain-rate (or the logarithm of strain-rate) (e.g. [15,27]). The use of normalized DIF reduces the influence of the material strength on the DIF formulae.

Over the past few decades, a large number of experiments have been performed in order to quantify strain-rate effects for concrete-like materials. More works have been reported on the compressive strength, for which experimental data are available up to strain-rates of around $10^3\ s^{-1}$, than on the tensile strength, for which publications can be found up to strain-rates around $10^2\ s^{-1}$. A thorough review of the dynamic tensile behaviours of concrete-like materials can be referred to, for example, [14,28]. Dynamic tensile testing results suggested that the strain-rate influence on the tensile strength becomes significant when the strain-rate is greater than a transition strain-rate in the range of 10^0–$10^1\ s^{-1}$ [2,7,8,14]. Based on the available experimental data and the use of various regression-analysis techniques, a number of curves have been proposed to describe the increase of tensile strength with strain-rate, which is discussed in this section.

European CEB recommended DIF formula for concrete in tension with strain-rates up to $300\ s^{-1}$ [29], which takes the following form

$$\mathrm{DIF} = \frac{\sigma_{td}}{\sigma_{ts}} = \begin{cases} 1 & \dot{\varepsilon}_z \le \dot{\varepsilon}_s \\ \left(\dot{\varepsilon}_z/\dot{\varepsilon}_s\right)^{1.016\alpha_s} & \dot{\varepsilon}_s < \dot{\varepsilon}_z \le 30\ s^{-1} \\ \gamma_s\left(\dot{\varepsilon}_z/\dot{\varepsilon}_s\right)^{0.33} & \dot{\varepsilon}_z > 30\ s^{-1} \end{cases} \tag{10}$$

where σ_{ts} and σ_{td} are the unconfined uniaxial tensile strengths in quasi-static and dynamic loading conditions, respectively; $\gamma_s = 10^{(7.11\alpha_s - 2.33)}$; $\alpha_s = 1/(10 + 6\sigma_{cs}/\sigma_{co})$; $\dot{\varepsilon}_s = 3 \times 10^{-6}\ s^{-1}$; $\sigma_{co} = 10$ MPa; σ_{cs} is the unconfined quasi-static uniaxial compressive strength (in MPa). Fig. 5 compares the CEB formula [Eq. (10)] when $\sigma_{cs} = 40$ MPa with the available experimental results in literature, which shows that the CEB tensile DIF substantially underestimates the tensile strain-rate effect.

Based on a review of experimental data of strain-rate effects on the tensile strength of concrete, following modification to the present CEB expression is suggested by Malvar and Crawford [30], i.e.

$$\mathrm{DIF} = \frac{\sigma_{td}}{\sigma_{ts}} = \begin{cases} 1 & \dot{\varepsilon}_z \le \dot{\varepsilon}_s \\ \left(\dot{\varepsilon}_z/\dot{\varepsilon}_s\right)^{\alpha_s} & \dot{\varepsilon}_s < \dot{\varepsilon}_z \le 1\ s^{-1} \\ \gamma_s\left(\dot{\varepsilon}_z/\dot{\varepsilon}_s\right)^{0.33} & \dot{\varepsilon}_z > 1\ s^{-1} \end{cases}, \tag{11}$$

in which

$\gamma_s = 10^{(6\alpha_s - 2)}$

$\alpha_s = 1/(1+8\sigma_{cs}/\sigma_{co})$ and

$\dot{\varepsilon}_s = 1 \times 10^{-6}\ s^{-1}$.

Zhou and Hao [31] recommended a tensile DIF curve for concrete-like materials, which is fitted from experimental results of [14,28], i.e.

$$\mathrm{DIF} = \frac{\sigma_{td}}{\sigma_{ts}} = \begin{cases} 1 & \dot{\varepsilon}_z \le 10^{-4}\ s^{-1} \\ 1 + 0.26\left[\lg\left(\dot{\varepsilon}_z\right) + 4.0769\right] & 10^{-4} < \dot{\varepsilon}_z \le 1\ s^{-1} \\ 1 + 2\left[\lg\left(\dot{\varepsilon}_z\right) + 0.53\right] & \dot{\varepsilon}_z > 1\ s^{-1} \end{cases}. \tag{12}$$

Based on the testing results of rocks, Zhou and Hao [3] suggested a tensile DIF formula for concrete aggregates, i.e.

$$\mathrm{DIF} = \frac{\sigma_{td}}{\sigma_{ts}} = \begin{cases} 1 + 0.0225\left[\lg\left(\dot{\varepsilon}_z\right) + 5.3333\right] & \dot{\varepsilon}_z \le 0.1\ s^{-1} \\ 1.6 + 0.7325\left[\lg\left(\dot{\varepsilon}_z\right)\right]^2 + 1.235\lg\left(\dot{\varepsilon}_z\right) & 0.1 < \dot{\varepsilon}_z \le 50\ s^{-1} \end{cases}. \tag{13}$$

A series of dynamic splitting tests have been conducted by Tedesco and Ross [8] for concrete specimens with different compressive strengths. Based on the results from these tests, a bilinear tensile DIF regression formula was suggested [8],

$$\mathrm{DIF} = \frac{\sigma_{td}}{\sigma_{ts}} = \begin{cases} 1 + 0.1425\left[\lg\left(\dot{\varepsilon}_z\right) + 5.8456\right] \ge 1.0 & \dot{\varepsilon}_z \le 2.32\ s^{-1} \\ 1 + 2.929\left[\lg\left(\dot{\varepsilon}_z\right) - 0.0635\right] \le 6.0 & \dot{\varepsilon}_z > 2.32\ s^{-1} \end{cases}. \tag{14}$$

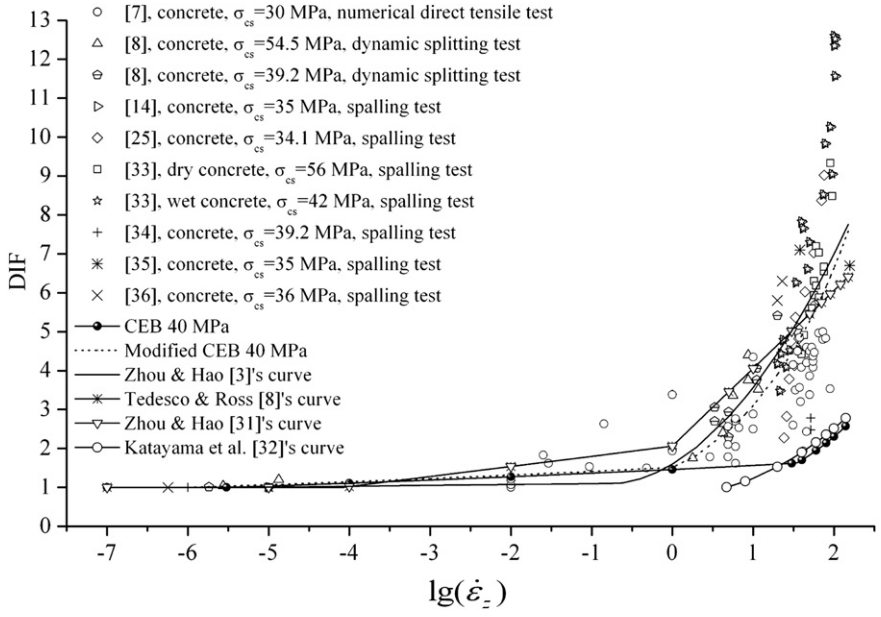

Fig. 5. Strain-rate influence on the tensile strength of concrete-like materials.

Katayama et al. [32] introduced a parabolic tensile DIF expression for concrete, i.e.

$$\mathrm{DIF} = \frac{\sigma_{\mathrm{td}}}{\sigma_{\mathrm{ts}}} = 0.4379\left[\lg(\dot{\varepsilon}_z)\right]^2 - 0.02987\lg(\dot{\varepsilon}_z) + 0.8267. \quad (15)$$

Above mentioned tensile DIF formulae, together with available experimental data, are shown in Fig. 5, which clearly indicates that there is a sharp increase of DIF beyond a transition strain-rate of around 10^0–$10^1\ \mathrm{s}^{-1}$ for concrete-like materials. Cotsovos and Pavlović [7] attributed the observed dynamic enhancement of tensile strength of concrete to "structural" effect while others (e.g. [2]) considered this as genuine material behaviour of concrete. In next section, we will apply the so-called "reconstitution method" through finite element (FE) simulations of three types of dynamic tensile tests to clarify this issue.

3. The "structural" effect on the dynamic tensile strength of concrete-like materials

3.1. Methodology

The "reconstitution method" is a numerical SHPB test introduced by Bertholf and Karnes [37] based on a finite difference (FD) code in order to investigate the "apparent strain-rate effects that do not represent real material behaviour" in a corresponding real SHPB test. In Ref. [37], SHPB pressure bars are modelled by FD elements with an isotropic elastic constitutive equation for the pressure bar material while the SHPB specimen is modelled as a strain-rate-independent material through the Levy–Mises plasticity model. In a numerical SHPB test, compressive loading can be applied either by the direct impact of the striking bar or the input of the measured stress pulse at the strain gauge station on the input pressure bar. In a laboratory SHPB test, incident, reflected and transmitted strain signals measured at strain gauge stations on input and output pressure bars are shifted to the interface between the SHPB specimen and the pressure bar. Then, SHPB formulae can be used to obtain the time variations of the average stress, strain and strain-rate within the SHPB specimen, based on which stress–strain relationship at various strain-rates can be obtained. Since the specimen material is treated to be strain-rate-independent in the numerical SHPB test, the observed apparent strain-rate effects represent "structural" effects rather than an inherent material strain-rate effect.

It should be noted that the so-called "structural" effects depend on the constitutive model used for the SHPB specimen. When the SHPB specimen material is described by a macroscopic, isotropic and homogenous constitutive model, the "structural" effects include the violations of SHPB test assumptions, e.g., the violation of uniaxial stress assumption due to the radial confinement introduced by interface friction and radial inertia effects and the violation of stress uniformity in SHPB specimen due to the axial inertia effect. However, if the SHPB specimen model includes micro-mechanisms (e.g. crack propagation, heterogeneity), the observed apparent strain-rate effects may represent real material behaviour in a macroscopic sense. Although this is not the case in the present study, other researchers (e.g. [7]) did mix up the "structural" effects with "micro-mechanism" effects. In the authors' opinion, the latter should be treated as real strain-rate effects of the tested material.

The "reconstitution method" has been used in several publications to investigate the "structural" effects in SHPB tests [1–6,38]. Meng and Li [38] and Lu and Li [39] recommended a procedure based on the "reconstitution method" to correct non-strain-rate effects, or "structural" effects, in SHPB tests.

In this section, the "reconstitution method" will be applied with finite element method to study the "structural" effect on the dynamic tensile strength of concrete-like materials in three types of dynamic tensile tests (i.e. direct dynamic tensile test, dynamic splitting test and spalling test), as shown in Fig. 6. Geometrical and material parameters of these experimental set-ups and specimens are taken from relevant publications, as shown in Table 1. Normalized input stress pulses for the direct dynamic tensile tests and dynamic splitting tests in Table 1 are illustrated in Fig. 7.

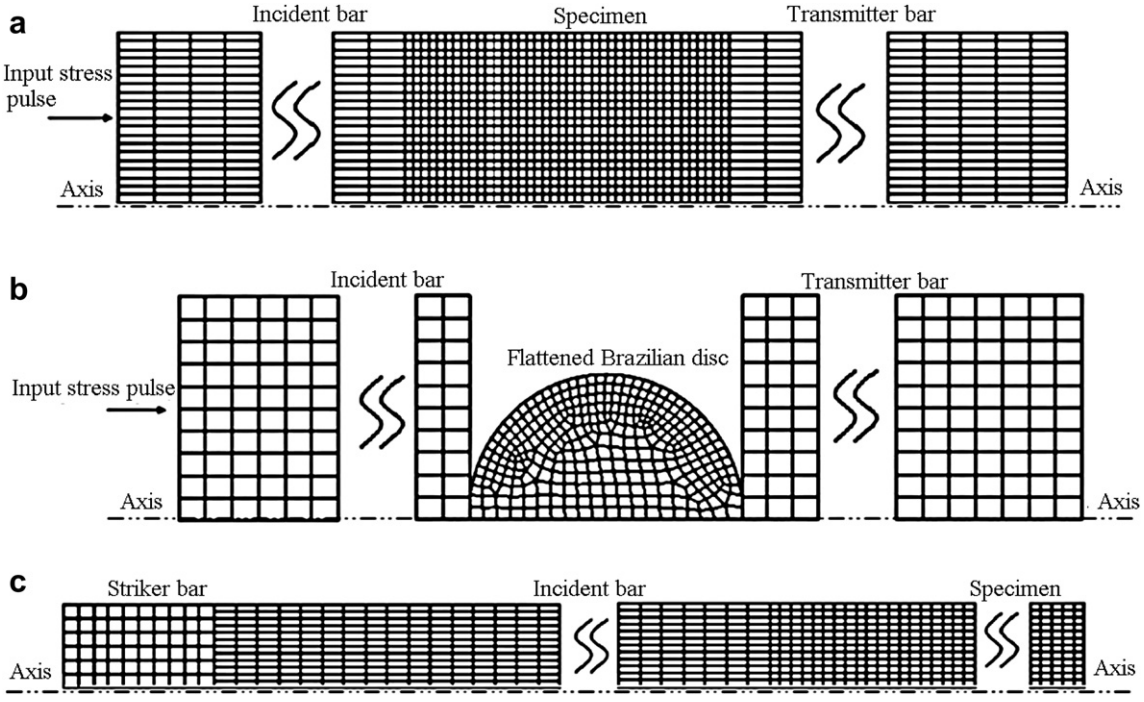

Fig. 6. Finite element models of (a) direct dynamic tensile tests, (b) dynamic splitting tests, and (c) spalling tests.

Table 1
Dimensions and material properties of dynamic tensile test set-ups and concrete samples.

	Dimensions		Material properties				Reference	Note
	Length (m)	Diameter (m)	Material	E (GPa)	ρ (kg/m^3)	ν		
Incident bar	3.35	0.0508	Steel	200	7800	0.35	[20]	Direct dynamic tensile tests with input stress pulse 1
Transmitted bar	3.66	0.0508						
Specimen	0.0508	0.0508	Concrete	20.3	2179	0.18		
Incident bar	4.5	0.1	Steel	200	7800	0.35	[13]	Dynamic splitting tests with input stress pulse 2
Transmitted bar	2.5	0.1						
Specimen	0.026	0.065	Concrete	20.3	2179	0.18		
Striker bar	0.08	0.04	Al 6060-T5	69.5	2700	0.32	[26]	Spalling tests with direct striking
Incident bar	1.0	0.04						
Specimen	0.12	0.04	Concrete	20.3	2179	0.18		

Various constitutive models have been developed for concrete-like materials and implemented in well-known computational codes, e.g. Drucker–Prager model in ABAQUS, K&C concrete model in LS-DYNA and RHT model in AUTODYN [40]. The K&C concrete model in LS-DYNA is used in this study to present our findings. It should be noted that the particular selection of the K&C concrete model does not restrain the generality of the findings and conclusions.

Specimens in these tests were modelled with the K&C concrete model (MAT_072) with an automatic model parameter generation capacity that is available in LS-DYNA version 971 [41]. A complete description of the model and validation is given in Ref. [27]. The quasi-static uniaxial tensile stress–strain relation of concrete can be described by an elastic regime before failure and a post-failure regime, as shown in Fig. 8. In the present study, the curve from Ref. [42] will be adopted as an example without losing generality, where the tensile and compressive strength of the concrete are 3.2 and 44.8 MPa, respectively.

In the K&C concrete model, we assume that material properties of concrete are independent of strain-rate. If the apparent tensile strength in numerical tensile tests increases with strain-rate, this should be contributed to "structural" effects, rather than strain-rate effects. In other words, if the "structural" effects do not exist in these dynamic tensile tests, the tensile strength obtained from these numerical simulations based on strain-rate-independent model will not vary with strain-rate.

3.2. Results and discussion

For numerical direct dynamic tensile tests on concrete specimens, an example of the reconstituted axial stress–strain curves at a strain-rate of 3.12 s^{-1} is shown in Fig. 9. It shows that the axial stress–strain curve fits the input uniaxial tensile stress–strain curve very well, especially before the ultimate tensile strength is reached. No apparent strain-rate effect on tensile strength is observed. When the average stress triaxiality obtained by spatially averaging the stress triaxiality over the entire specimen elements is examined, it is found that stress triaxiality is about 1/3 of the corresponding axial tensile stress. It transpires that other two principal stresses (i.e. the radial stress shown in Fig. 10) are both very small and the stress state in majority of the specimen material is uniaxial in these numerical simulations of direct dynamic tensile tests.

The stress state within the elements located near the central line along the vertical diameter of concrete samples in dynamic splitting tests is multi-axial, as shown in Fig. 11. However, no "structural" effects on the dynamic tensile strength are observed in numerical dynamic splitting tests. The apparent DIF of concrete samples obtained from direct dynamic tensile tests and dynamic splitting tests are presented in Fig. 12. Experimental results of these two types of tensile tests from independent publications are also presented for comparison purpose. It is found that the numerically predicted DIFs are generally independent of strain-rate, and thus, it is concluded that the dynamic tensile strength enhancement of concrete-like materials is attributed to the strain-rate effect at macroscopic level.

Based on results obtained from numerical simulations of spalling tests (e.g. Fig. 13), values of tensile strength under various strain-rates are obtained from Eqs. (8) and (9) according to [14,24]. The numerically predicted uniaxial tensile strength in spalling tests is almost independent of strain-rate, as shown in Fig. 14, where dynamic uniaxial tensile strength from spalling experiments are

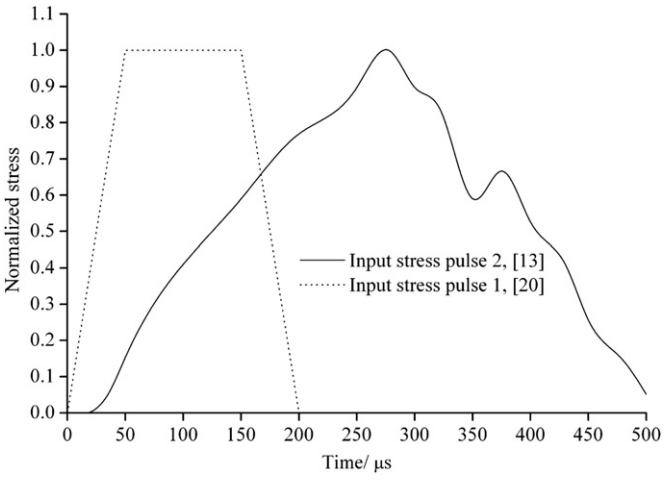

Fig. 7. Normalized input stress pulses used in the FE simulations of direct dynamic tensile tests (input stress pulse 1) and dynamic splitting tests (input stress pulse 2).

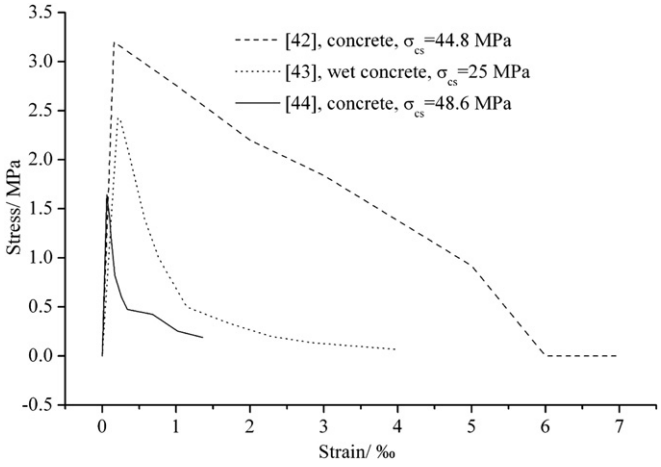

Fig. 8. Typical uniaxial tensile stress–strain relations of concrete.

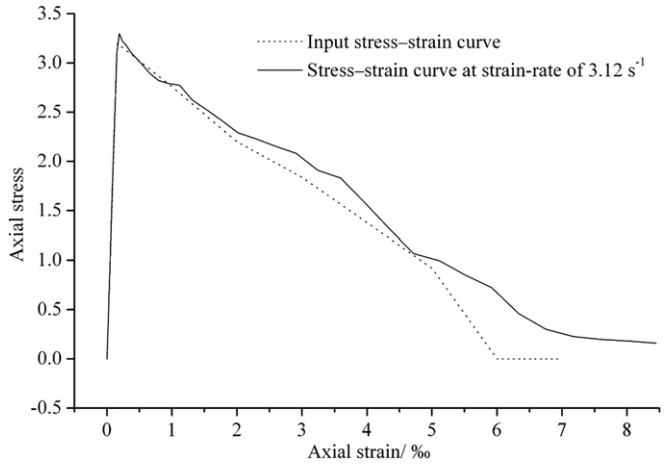

Fig. 9. An axial stress–strain curve predicted from simulations of direct dynamic tensile tests.

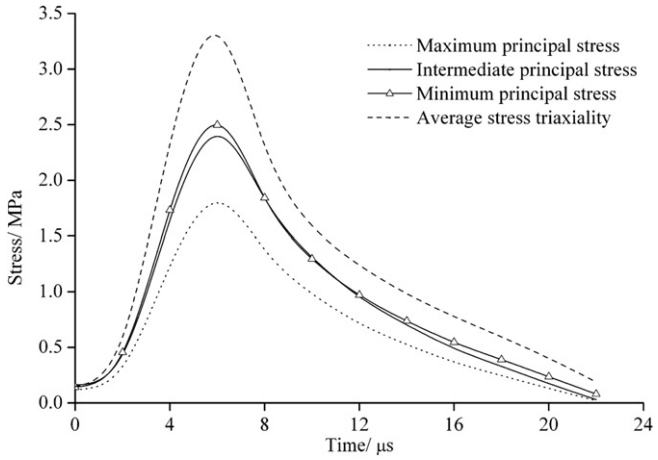

Fig. 11. The stress state within the elements located near the central line along the vertical diameter of concrete samples in dynamic splitting tests at a strain-rate of 18.3 s^{-1}.

also included for comparison purpose. The stress state in the spalling test sample is uniaxial. Therefore, we conclude that the tensile DIFs from spalling tests can also represent the strain-rate effect on the tensile strength of concrete-like materials, which agrees with the findings in Ref. [2].

4. A micro-mechanism model for the dynamic tensile strength of concrete-like materials

The weak strain-rate sensitivity of concrete-like materials under both tension and compression within the range of strain-rates up to about 10^0 s^{-1} is attributed to the free water present inside the nano-pores of the material. The water content causes an internal viscosity and delays crack propagation (e.g. [46,50–55]). On the other hand, when the strain-rate is above the transition strain-rate (10^0–10^1 s^{-1}), the free water content plays little role on the strain-rate sensitivity of tensile strength (e.g. [21,46]). Thus, the physical source of the strain-rate sensitivity of tensile strength at moderate to high strain-rates for concrete-like materials is mainly due to other physical phenomena rather than the free water content [33].

At mesoscale, concrete is regarded as a three-phase composite material consisting of different sized aggregate particles, mortar matrix (including small sand particles bonded by cement paste) and interfaces between the aggregate and the mortar matrix. From the viewpoint of micro-mechanisms, one of the most important factors that may affect the dynamic behaviour of brittle materials is their heterogeneity. It has been found that the heterogeneity of rocks contributes to the difference between the dynamic and static tensile strengths, i.e. an increase in the heterogeneity coefficient leads to an increase in the strain-rate dependency (e.g. [56,57]). The influence of the material heterogeneity on the tensile strength of concrete-like materials will not be considered in the present study although it is likely to be one of the micro-mechanisms responsible for the observed strain-rate sensitivity of tensile strength of concrete-like materials.

Another micro-mechanism which may influence the strength of concrete-like materials is microcracks. For a typical pre-existing crack with initial length of $2c$ and oriented at an angle of β with respect to the axial direction, when an external tensile stress of σ_z is applied along the longitudinal direction of the specimen, the local Mode-I stress intensity factor (SIF) at the crack tips is given by [58]

$$K_{\mathrm{I}} = \sigma_z \cos^2 \beta \sqrt{\pi c}. \tag{16}$$

As the external uniaxial tensile stress σ_z increases, a point is reached at which the preferential cracks ($\beta = 0°$) start propagating

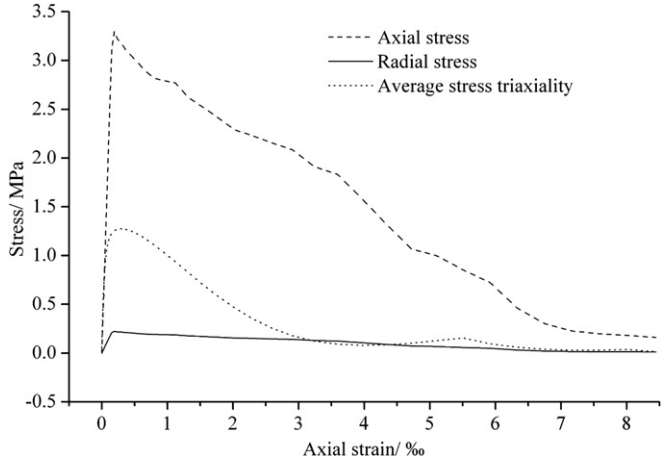

Fig. 10. The axial, radial stresses and average stress triaxiality versus the axial strain for concrete samples from numerical simulations of direct dynamic tensile tests at strain-rate of 3.12 s^{-1}.

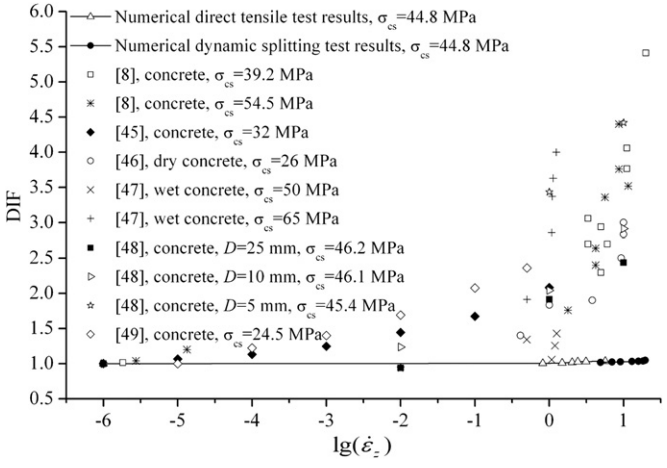

Fig. 12. Comparison of predicted numerical DIFs with experimental ones for direct dynamic tensile tests and dynamic splitting tests, where D is the effective diameter of concrete aggregates.

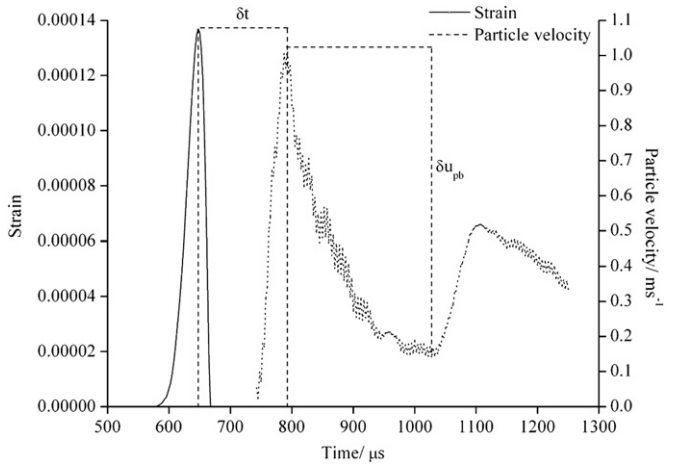

Fig. 13. Strain at the incident bar/specimen interface and particle velocity at the end of the specimen (δt is the time that the wave needs to propagate one specimen length).

unstably and failure of the entire specimen is imminent at this point. For a single, isolated crack, the critical stress at which this occurs is given by

$$\sigma_z = K_{IC}/\sqrt{\pi c}. \tag{17}$$

in which K_{IC} is the quasi-static fracture toughness.

Because of the existence of large number of microcracks, interactions among these cracks happen. Eq. (17) does not consider crack interaction, and thus, overestimates the overall failure stress of the specimen. For the microcrack array with equal orientation of $\beta = 0^\circ$, length of $2c$ and crack spacing of $2b$, the ultimate uniaxial tensile strength (σ_{ts}) can be calculated from the following expression with taking crack interaction into account [58]

$$\sigma_{ts} = K_{IC}\left(2b\tan\frac{\pi c}{(2b)}\right)^{-0.5}. \tag{18}$$

Above analysis may be further improved by introducing probability distribution functions for microcrack size and orientation for the prediction of the overall failure stress, which, however, will not be persuaded in this qualitative study in order to keep the simplicity of the problem.

According to Ref. [59], the Mode-I dynamic SIF of a crack array under uniformly distributed far-field uniaxial tensile loading with an instantaneous growth speed $\dot{l}(t)$ of the crack, can be related to the static SIF of an equivalent stationary crack array at the same instantaneous crack length $l(t)$ by,

$$K_{Id}^{array} = k(\dot{l})K_I^{array} \tag{19}$$

where $K_I^{array} = \sigma_z\sqrt{2b\tan(\pi l/2b)}$ according to Eq. (18), and $k(\dot{l})$, which represents the inertia effect on the SIF during dynamic crack growth, is suggested by Ref. [59] as

$$k(\dot{l}) = \frac{c_r - \dot{l}}{c_r - 0.5\dot{l}} \tag{20}$$

in which $c_r = [(0.862 + 1.14\nu_s)/(1+\nu_s)]\sqrt{E_s/[2(1+\nu_s)\rho_s]}$ is the Rayleigh wave speed with ν_s and ρ_s being the Poisson's ratio and density of the material.

Using the Irwin crack growth criteria (e.g. [60]), i.e., the cracks begin to propagate when K_{Id}^{array} reaches the critical SIF (also called dynamic fracture toughness) K_{IC}^{d}, and assuming that K_{IC}^{d} of the specimen material does not vary with strain-rate [60–62], i.e., $K_{IC}^{d} = K_{IC} =$ constant, then the dynamic crack growth criterion can be written as

$$K_{Id}^{array} = K_{IC}. \tag{21}$$

Combining Eqs. (19)–(21), the crack growth speed becomes

$$\dot{l} = c_r\frac{K_I^{array} - K_{IC}}{K_I^{array} - 0.5K_{IC}}. \tag{22}$$

The crack length is calculated by integrating the crack growth speed until either failure (i.e. the cracks coalesce when $l = b$) or complete unloading is attained. To obtain the failure stress for a given stress pulse under a constant strain-rate (i.e. a triangular stress pulse of $\sigma_z = E_s\dot{\varepsilon}_z t$ as has been used by Refs. [61–63]) and the material microstructure, we estimate the failure time t_f from $l = b$. Thus, t_f is given by

$$b = \int_0^{t_f}\dot{l}dt. \tag{23}$$

Then, the DIF of dynamic tensile strength can be deduced from

$$\mathrm{DIF} = \sigma_z\left(t_f\right)/\sigma_{ts} \tag{24}$$

where σ_{ts} is the quasi-static tensile strength given by Eq. (18).

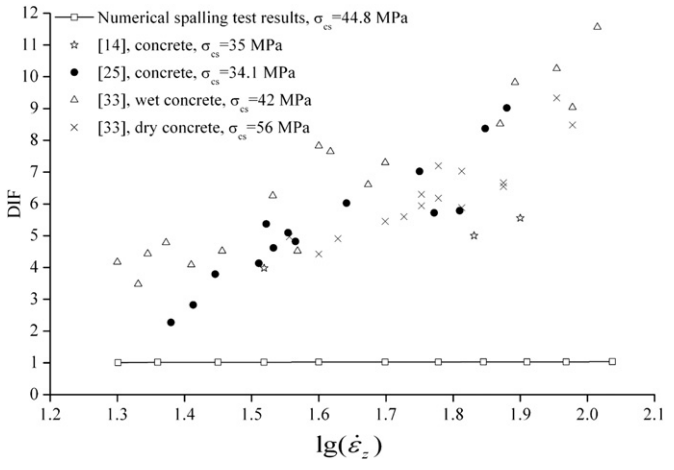

Fig. 14. Comparison of the predicted numerical DIFs with experimental ones for spalling tests.

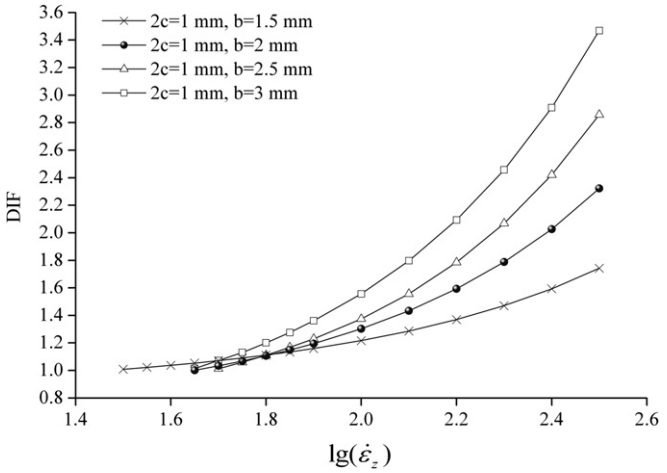

Fig. 15. The effect of microcrack spacing b on tensile strength.

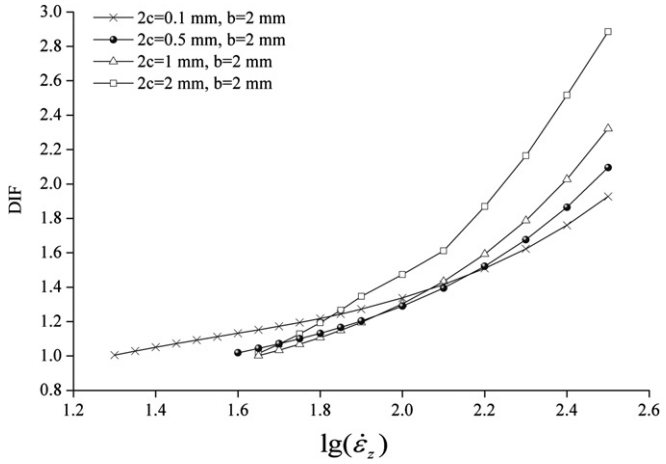

Fig. 16. The effect of microcrack size 2*c* on tensile strength.

As has been pointed out in Ref. [62], the assumption of a uniform far-field stress, which simplifies the calculation of the Mode-I dynamic SIF [i.e. Eq. (19)] for a crack array, should be satisfied for the validity of the model. According to Ref. [62], the limitation of the model is that the variation of the maximum applied stress normalized by the Young's modulus across the crack array, $\Delta\sigma_z/E_s = \dot{\varepsilon}_z L^*/c_s$ (in which L^* is the representative length of the crack array), should be smaller than 0.1.

In following examples of parametric analyses, typical material parameters of mortar are used, i.e., $E_s = 20.3$ GPa, $\nu_s = 0.18$, $\rho_s = 2179$ kg/m^3, and $K_{IC} = 0.5$ MPa$\sqrt{m}$. The tensile strength under uniaxial tensile loading is plotted as a function of the strain-rate in Fig. 15 for different values of the microcrack spacing *b* and a fixed value of the microcrack size 2*c*, and in Fig. 16 for various values of 2*c* and a fixed value of *b*. It is shown that the tensile strength generally increases with *b* at the same strain-rate when the microcrack size is fixed. For a given value of microcrack spacing *b*, the tensile strength decreases with microcrack size at low strain-rates, but increases with *b* at high strain-rates, which agree with the results shown in [17,31,55]. For all parameters examined in this study, the DIF increases with strain-rate in the moderate to high strain-rate regimes, which implies that microcrack inertia is one of the mechanisms responsible for the strain-rate sensitivity of the tensile strength of concrete-like materials.

It should be noted that the micro-mechanism model proposed in this section is also applicable to other brittle materials. For example, when applying this model to concrete specimens, the microcrack spacing 2*b* can be replaced by $2b = 2D_m(1 - V_f)/(3V_f) + D_m$ (where D_m is the diameter of the maximum size aggregate in concrete specimen and V_f is the volume fraction of coarse aggregate) [58]. The fracture criterion for a concrete specimen is expressed as $K_{Id}^{array} = K_{IC}^{a}$ (in which K_{IC}^{a} is the Mode-I fracture toughness of aggregates). However, the proposed model can only qualitatively illustrate the influence of microcrack inertia on the strain-rate sensitivity of concrete-like materials. Therefore, a multi-scale modelling with considering the micro-mechanisms of both material property heterogeneity and microcrack intertia should be performed to fully understand the dynamic tensile strength enhancement in concrete-like materials.

5. Conclusions

Numerical simulations of direct dynamic tensile tests, dynamic splitting tests and spalling tests based on a homogeneous strain-rate-independent model were performed on concrete. The effect of stress triaxiality on the dynamic tensile strength enhancement of concrete obtained from numerical dynamic splitting tests is found to be negligible. The stress state within the sample of a direct dynamic tensile test or a spalling test is dominated by a uniaxial stress state. Therefore, at macroscopic level, the apparent dynamic tensile strength enhancement observed in dynamic tensile tests is associated with intrinsic material properties, rather than "structural" effects. A micro-mechanism model based on dynamic fracture mechanics is presented. It shows that the observed increase of tensile strength with strain-rate from dynamic tensile tests can be largely attributed to the inertia effects of microcracks.

Acknowledgements

First author acknowledges the studentship from the School of Mechanical, Aerospace and Civil Engineering, The University of Manchester and the scholarship from Henry Lester Trust.

References

[1] Li QM, Meng H. About the dynamic strength enhancement of concrete-like materials in a SHPB. Int J Solids Struct 2003;40:343–60.
[2] Hentz S, Donzé FV, Daudeville L. Discrete element modelling of concrete submitted to dynamic loading at high strain rates. Comput Struct 2004;82:2509–24.
[3] Zhou XQ, Hao H. Modelling of compressive behaviour of concrete-like materials at high strain rate. Int J Solids Struct 2008;45:4648–61.
[4] Zhang M, Wu HJ, Li QM, Huang FL. Further investigation on the dynamic compressive strength enhancement of concrete-like materials based on split Hopkinson pressure bar tests part I: experiments. Int J Impact Eng 2009;36:1327–34.
[5] Li QM, Lu YB, Meng H. Further investigation on the dynamic compressive strength enhancement of concrete-like materials based on split Hopkinson pressure bar tests, part II: numerical simulations. Int J Impact Eng 2009;36:1335–45.
[6] Kim DJ, Sirijaroonchai K, El-Tawil SE, Naaman A. Numerical simulation of the split Hopkinson pressure bar test technique for concrete under compression. Int J Impact Eng 2010;37:141–9.
[7] Cotsovos DM, Pavlović MN. Numerical investigation of concrete subjected to high rates of uniaxial tensile loading. Int J Impact Eng 2008;35:319–35.
[8] Tedesco JW, Ross CA. Strain-rate-dependent constitutive equations for concrete. ASME J Press Vessel Technol 1998;120:398–405.
[9] Neville AM. Properties of concrete (Fourth edition). Harlow, England: Pearson Education Limited; 1995. p. 598–9.
[10] Kupfer J, Hilsdorf HK, Rusch H. Behavior of concrete under biaxial stresses. Am Concr Inst J 1969;66:656–66.
[11] ASTM. Standard test method for splitting tensile strength of cylindrical concrete specimens, ASTM C496-86, Annual book of standards. American Society for Testing Materials; 1986. 256–259.
[12] Galvez F, Sanchez Galvez S. Numerical modelling of SHPB splitting tests. J Phys IV 2003;110:347–52.
[13] Wang QZ, Li W, Xie HP. Dynamic split tensile test of flattened Brazilian disc of rock with SHPB setup. Mech Mater 2009;41:252–60.
[14] Schuler H, Mayrhofer C, Thoma K. Spall experiments for the measurement of the tensile strength and fracture energy of concrete at high strain rates. Int J Impact Eng 2006;32:1635–50.
[15] Tedesco JW, Powell JC, Ross CA, Hughes ML. A strain-rate-dependent concrete material model for ADINA. Comput Struct 1997;64:1053–67.
[16] Albertini C, Cadoni E, Labibes K. Study of the mechanical properties of plain concrete under dynamic loading. Exp Mech 1999;39:137–41.
[17] Cadoni E, Solomos G, Albertini C. Mechanical characterisation of concrete in tension and compression at high strain rate using a modified Hopkinson bar. Mag Concr Res 2009;61:221–30.
[18] Reinhardt HW. Concrete under impact loading-tensile strength and bond. Heron 1982;27:1–48.
[19] Reinhardt HW, Rossi P, van Mier JGM. Joint investigation of concrete at high rates of loading. Mater Struct 1990;23:213–6.
[20] Tedesco JW, Ross CA, Mcgill PB, O'Neil BP. Numerical analysis of high strain rate concrete direct tension tests. Comput Struct 1991;40:313–27.
[21] Zielinski AJ. Fracture of concrete and mortar under uniaxial impact tensile loading. Doctoral thesis, Delft University of Technology, The Netherlands; 1982.
[22] Ross CA, Tedesco JW, Kuenen ST. Effects of strain rate on concrete strength. ACI Mater J 1995;92:37–47.
[23] London JW, Quinney H. Experiment with the pressure Hopkinson bar. Proc R Soc London A Math Phys Sci A 1923;103:622–43.
[24] Gálvez Díaz-Rubio F, Rodríguez Pérez J, Sánchez Gálvez V. The spalling of long bars as a reliable method of measuring the dynamic tensile strength of ceramics. Int J Impact Eng 2002;27:161–77.

[25] Wu HJ, Zhang QM, Huang FL, Jin QK. Experimental and numerical investigation on the dynamic tensile strength of concrete. Int J Impact Eng 2005;32:605–17.
[26] Klepaczko JR, Brara A. An experimental method for dynamic tensile testing of concrete by spalling. Int J Impact Eng 2001;25:387–409.
[27] Malvar LJ, Crawford JE, Wesevich JW, Simons D. A plasticity concrete material model for DYNA3D. Int J Impact Eng 1997;19:847–73.
[28] Malvar LJ, Ross CA. Review of strain rate effects for concrete in tension. ACI Mater J 1998;95:735–9.
[29] Comite Euro-International du Beton. CEB-FIP model code 1990. Trowbridge, Wiltshire, UK: Redwood Books; 1993.
[30] Malvar LJ, Crawford JE. Dynamic increase factors for concrete. In: 28th Department of Defense Explosives Safety seminar, Orlando, FL; August 1998. p. 1–17.
[31] Zhou XQ, Hao H. Mesoscale modelling of concrete tensile failure mechanism at high strain rates. Comput Struct 2008;86:2013–26.
[32] Katayama M, Itoh M, Tamura S, Beppu M, Ohno T. Numerical analysis method for the RC and geological structures subjected to extreme loading by energetic materials. Int J Impact Eng 2007;34:1546–61.
[33] Brara A, Klepaczko JR. Experimental characterization of concrete in dynamic tension. Mech Mater 2006;38:253–67.
[34] Cadoni E, Labibes K, Berra M, Giangrasso M, Albertini C. High-strain-rate tensile behaviour of concrete. Mag Concr Res 2000;52:365–70.
[35] McVay MK. Spall damage of concrete structures, Technical report SL-88-22. Waterways Experiment Station, Vicksburg, MS: U.S. Army Corps of Engineers; June 1988.
[36] Mellinger FM, Birkimer DL. Measurement of stress and strain on cylindrical test specimens of rock and concrete under impact loading, Technical report 4-46. Cincinnati, Ohio: U.S. Army Corps of Engineers, Ohio River Division Laboratories; April 1966. p. 71.
[37] Bertholf LD, Karnes CH. Two dimensional analysis of the split Hopkinson pressure bar system. J Mech Phys Solids 1975;23:1–19.
[38] Meng H, Li QM. Correlation between the accuracy of a SHPB test and the stress uniformity based on numerical experiments. Int J Impact Eng 2003;28:537–55.
[39] Lu YB, Li QM. Determination of strain-rate effect on the compressive strength of brittle materials based on SHPB testing. No. 49. In: Li QM, Hao H, Li ZX, Yankelevsky D, editors. Proceedings of the First International Conference of Protective Structures; 2010. p. 1–8. Manchester.
[40] Li QM, Reid SR, Wen HM, Telford AR. Local impact effects of hard missiles on concrete targets. Int J Impact Eng 2005;32:224–84.
[41] LS-DYNA. Keyword user's manual, version 971, vol. I. Livermore Software Technology Corporation; 2007. 1650–1657.
[42] Noble C, Kokko E, Darnell I, Dunn T, Hagler L, Leininger L. Concrete model descriptions and summary of benchmark studies for blast effects simulations, U.S Department of Energy Report No. UCRL-TR-215024; 2005. p. 246.
[43] Freund LB. Dynamic fracture mechanics. Cambridge Monographs on Mechanics and Applied Mechanics. In: Bachelor GK, Wunsch C, Rice J, editors. Cambridge, UK: Cambridge University Press; 1998. p. 313–39.
[44] Reinhardt HW, Cornelissen HAW, Hordijk DA. Tensile tests and failure analysis of concrete. J Struct Eng 1986;112:2462–77.
[45] Faria R, Oliver J, Cervera M. A strain-based plastic viscous-damage model for massive concrete structures. Int J Solids Struct 1998;35:1533–58.
[46] Ross CA, Jerome DM, Tedesco JW, Hugues ML. Moisture and strain rate effects on concrete strength. ACI Mater J 1996;93:293–300.
[47] Le Nard H, Bailly P. Dynamic behaviour of concrete: the structural effects on compressive strength increase. Mech Cohesive Frict Mater 2000;5:491–510.
[48] Cadoni E, Labibes K, Berra M, Giangrasso M, Albertini C. Influence of aggregate size on strain-rate tensile behavior of concrete. ACI Mater J 2001;98:220–3.
[49] Yan DM, Lin G. Dynamic properties of concrete in direct tension. Cem Concr Res 2006;36:1371–8.
[50] Rossi P, Boulay C. Influence of free water in concrete on the cracking process. Mag Concr Res 1990;42:143–6.
[51] Rossi P. Influence of cracking in the presence of free water on mechanical behaviour of concrete. Mag Concr Res 1991;43:53–7.
[52] Rossi P. A physical phenomenon which can explain the mechanical behaviour of concrete under high strain rates. Mater Struct 1991;24:422–4.
[53] Rossi P, van Mier JGM, Boulay C, Le Maou F. The dynamic behaviour of concrete: influence of free water. Mater Struct 1992;25:509–14.
[54] Rossi P, Toutlemonde F. Effect of loading rate on the tensile behaviour of concrete: description of the physical mechanisms. Mater Struct 1996;29:116–8.
[55] Cadoni E, Labibes K, Albertini C, Berra M, Giangrasso M. Strain-rate effect on the tensile behaviour of concrete at different relative humidity levels. Mater Struct 2001;34:21–6.
[56] Cho SH, Ogata YJ, Kaneko K. Strain-rate dependency of the dynamic tensile strength of rock. Int J Rock Mech Min Sci 2003;40:763–77.
[57] Ma GW, Wang XJ, Li QM. Modeling strain-rate effect of heterogeneous materials using SPH method. Rock Mech Rock Eng 2010;43:763–76.
[58] Fanella DA. Fracture and failure of concrete in uniaxial and biaxial loading. J Eng Mech 1990;116:2341–62.
[59] Freund LB. Dynamic fracture mechanics. Cambridge: Cambridge University Press; 1990.
[60] Paliwal B, Ramesh KT. An interacting micro-crack damage model for failure of brittle materials under compression. J Mech Phys Solids 2008;56:896–923.
[61] Huang C, Subhash G. Influence of lateral confinement on dynamic damage evolution during uniaxial compressive response of brittle solids. J Mech Phys Solids 2003;51:1089–105.
[62] Nemat-Nasser S, Deng H. Strain-rate effect on brittle failure in compression. Acta Metall Mater 1994;42:1013–24.
[63] Ravichandran G, Subhash G. A micromechanical model for high strain rate behavior of ceramics. Int J Solids Struct 1995;32:2627–46.